COPPER AT SILICA CORE - SHELL NANOPARTICLES AS ANTIBACTERIAL AGENTS BY SOL-GEL CHEMICAL METHODS

Al- Ajeeli, Alaa F. Hashim

Department of Physics, College of Education for Pure Sciences, Tikrit University, Salahuddin, Iraq

alaa.f.hashim@st.tu.edu.iq - https://orcid.org/0000-0003-3688-0663

Razeg, Khalid Hamdi

Department of Physics, College of Education for Pure Sciences, Tikrit University, Salahuddin, Iraq

khalid.hr55@tu.edu.iq

Fuad Tariq Ibrahim

Department of Physics, College of Science, University of Baghdad, Baghdad, Iraq

Reception: 24/11/2022 **Acceptance**: 09/01/2023 **Publication**: 02/02/2023

Suggested citation:

A. A., Alaa F. Hashim, R., Khalid Hamdi and F. T., Ibrahim, (2023). **Copper At Silica Core - Shell Nanoparticles As Antibacterial Agents By Sol-Gel Chemical Methods.** *3C Tecnología. Glosas de innovación aplicada a la pyme, 12(1)*, 337-352. https://doi.org/10.17993/3ctecno.2023.v12n1e43.337-352

ABSTRACT

Core-shell Cu@sio2 nanoparticles were created by a chemical reaction in a sol gel, and their ability to inhibit S. aureus and E. coli bacteria was tested, when synthesized and characterized using ultraviolet-visible spectroscopy, a copper band could be seen before and after encapsulation at wavelengths of 625 nanometers and 635 nanometers, which are surface plasmonic resonant frequency bands, respectively. The production of Cu @Sio2 core shell nanoparticles was further confirmed using field emission scanning electron microscope (FESEM) pictures. The core shell nanoparticles have a mean size of 66 nanometers and a spherical shape, as shown in TEM. The X-ray diffraction patterns for the nanoparticles, which show face-centered cubic (FCC) of copper, match the crystal structure of Cu@sio2 we discovered using fourier transform infrared (FT-IR) spectroscopy, the fourier transform infrared interaction between the silica and the synthesized copper NPs was investigated. This revealed the capping of the CuNPs by SiO2. The inhibition zone was evident as a result of the activities of these compounds (14, 14, 16, and 20) and (24, 24, 28, and 30) against Escherichia coli bacteria and Staphylococcus aureus bacteria, respectively.

KEYWORDS

Copper Nanoparticle, Silica, Antibacterial, Inhibition Zone.

https://doi.org/10.17993/3ctecno.2023.v12n1e43.337-352

PAPER INDEX

https://doi.org/10.17993/3ctecno.2023.v12n1e43.337-352

1. INTRODUCTION

The modern concepts for producing nanoparticles with the required size and form are developing as, science and technology grow more quickly, particularly in the fields of nanotechnology and material science. [1-4] Metallic nanoparticles are gaining popularity due to their different physical and chemical characteristics, as well as their wide variety of applications. There is an increase in interest in working with metals, polymer particles, metallic nanoparticles, etc. because of they have several applications in material science due to their tiny size and a huge interaction surface. surrounding medium affects the features of nanoparticles, and the necessary attributes can be introduced by changing the ambiance. The scientific discipline of nanotechnology has enormous promise for use in medicine. Because nanoscience and biology are comparable to nature, their combination will not only help in the battle against harmful microbes, but may also lead to a shift in how infectious disease is treated. [5] [6] Numerous biomedical, and pharmaceutical fields, including diagnostics, genetic engineering, drug delivery, biomarkers, bioimaging, cosmetics, antibacterial, cancer, immunology, cardiology, cancer treatment, bioremediation, water treatments, energy production, and other infectious diseases, can benefit from the use of nanoparticles. [7-9] Paints typically contain different metals and metal oxides as NPs because they have antifungal, anti-algal, and antibacterial effects. Exhibiting water resilience, fewer toxic effects, and antibacterial capabilities through attaching to bacterial cell proteins. [10]

There are generally two ways to synthesize nanoparticles of Sio_2. Since silica has been widely used as an efficient anticorrosive protective material, numerous attempts have been made to coat metal nanoparticles with silica shells of customizable thickness. Due to its excellent compatibility with various materials, great chemical and thermal stability, and huge surface area, silica is a very important material. SiO_2 with copper exhibited excellent corrosion resistance [11] Multi-infectious bacteria can produce antimicrobial resistance by adhering to various substrates like medical equipment or biological surfaces like host organism and forming sticky exopolymeric substances (EPS) called microbial biofilms [12].

Copper nanoparticles are reported to be more efficient than iron oxide and nickel nanoparticles in the attack against pathogenic bacteria that produce biofilms and multidrug resistance. Copper and copper oxide nanoparticles exhibit antibacterial efficacy against the microorganism's Staph aureus, E. coli, Pseudomonas aerugi, and B. subtilis the microorganism's Bacillus nosa that produce biofilms. [13-16].

Copper nanoparticles are useful for a variety of purposes, including medicinal, agricultural, and other industries, and they are inexpensive, these include antifungal, antiviral, antibiotic, anticancer, and photocatalytic uses[17].

In this study, $Cu@Sio_2$ core-shell nanoparticles are fabricated using the chemical sol-gel method [18-19]. Ultrasound is used to disperse copper nanoparticles before mixing them with silica. The final spherical $Cu@Sio_2$ core -shell the spherical shape was observed as well as measuring the antibacterial activities of Escherichia coli and Staphylococcus aureus bacteria.

https://doi.org/10.17993/3ctecno.2023.v12n1e43.337-352

2. EXPERIMENTAL PARTS

2.1. SOL-GEL PROCESS

Synthesis of Copper Nanopowder in Chemical Sol Gel (average particle size 30 nanometer ≥99.9%), (TEOS) tetraethylorthosilicate 98%, 0.5 mol (Merck), ethyl alcohol (99.9%), ascorbic acid (99%), cetyltrimethylammonium bromide ≥98%, NH3 ammonium hydrate (25%), also utilized was deionized water.

Experiment was carried out 24C° temperature. Shows the composition of core-shell used in the experiment. The technique of synthesizing core-shell is as follows. First, the copper solution is made up of 180 mg of Cu nanopowder combined with 10 ml of distilled water, (0.004 M) cetyltrimethylammonium bromide (CTAB) diluted in 10 ml of water, and (0.02 M) ascorbic acid mixed in 20 ml of water. and fully dispersed with ultrasound. Then, while stirring, 32.0 ml of ethanol and 0.5 ml of TEOS were combined. 1.5 ml of ammonium hydroxide was combined after stirring for around one hour and the reaction was then completed after another 24 hours of stirring. The core-shell nanoparticles underwent multiple filtering and washing steps using distilled water and ethanol.lastlly,80 °C was used to dry powder to produce Cu@sio2 core-shell.

2.2. CHARACTERIZATION TECHNIQUES

Utilizing X-ray diffraction, Cu@SiO_2 core-shell peaks were verified. (XRD; Cu, 30 kV, 15 milliampere); Rigaku Corporation), To make specimens, the sol-gel-fabricated core-shells were disseminated in ethanol. The core-shell shapes were verified using a transmission electron microscope and fesem. Then, measurements using energy dispersive X-ray spectroscopy (EDS) produced to confirm the production of the SiO2 shell and Copper nanopowder core. The following techniques were used to characterize the prepared Cu @Sio_2 core shell nanostructures.

2.3. EQUATIONS USED TO ANALYSIS THE XRAY RESULTS.

According to the findings of the XRD examination, the Bragg law Equation (1) was used to compute the d-spacing (the lattice planes distance between the atoms), and the Debye-Scherrer Equation was used to calculate the average crystallite size. (2)

$$2d\ sin\theta = n\lambda \tag{1}$$

where d is the interplanar distance between atoms, n is an integer (n= 1), and k is an integer (k= 0.15418 nanometer for Cu Ka).

$$D = \frac{K\lambda}{FWHM\ COS\theta} \tag{2}$$

where K is a constant number factor (0.89), λ= 0.15418 nanometers for Cu Ka, FWHM is the full width at half maximum, θ is the diffraction angle, and (a) is the lattice constant, while D is the average crystallite size. (a) For cubic crystals was calculated by Equation (3) [17]

https://doi.org/10.17993/3ctecno.2023.v12n1e43.337-352

$$a = d\sqrt{h^2 + k^2 + l^2} \quad (3)$$

Miller's index (h k l) represents cartesian coordinates for cubic crystals.

2.4. TESTING FOR ANTIMICROBIAL EFFECTIVENESS

The antibacterial capabilities of the composite membrane were tested using the diffusion method against the gram-positive bacterium. Staphylococcus aureus and gram-negative bacteria a kind of bacteria called Escherichia coli. [20]. A disk-shaped test specimen and an untreated control were created with a 10 mm diameter and sterilized in an autoclave for 15 minutes at 120 °C for the disk diffusion procedure. After that, they were placed on individual agar media with E. coli and S. aureus cultures and for 24 hours at 37 °C while the inhibitory zone was monitored.

3. 3. RESULTS AND DISCUSSION

3.1. X-RAY DIFFRACTION

Among the most effective and simple methods for determining out a compound's crystallite properties is X-ray diffraction (XRD). XRD analysis of synthesized copper nanopowder using ascorbic acid and CTAB as stabilizing and reduction agents, confirmed that the finished item is made of metal. The Cu-NPs' XRD patterns are depicted in Fig. 1, and they are very comparable to those seen in JCPDS Copper. 04-0836 (43.6, 50.8, and 74.4) correspond to the metallic Cu planes (111), (200), and (220). The outcome of XRD examination shows that the produced Cu-NPs have a face-centered cubic structure (FCC), in addition to copper peaks, other X-ray diffraction peaks appear after the process of coating the metal with silica figure 2 depicts the Cu@sio2 core shell's XRD pattern. nanostructure as it was created using the sol-gel process. Peaks seen at 2θ values of 21.4, 22.59, 31.8, 45.54, 53.97, 54.55, 56.6, 66.15 and 75.47 correspond to (002), (211), (600), (332), (440),(404), (620),(325)and (435) planes of Cu@Sio_2. These peaks were quite comparable to those of the standard JCPDS Card No. 045-0131 for the sio2 [21].

The JCPDS (Joint Committee on Powder Diffraction Standards) was used to calculate the broadening of the diffraction peaks matching to the strongest reflections, which indicates the mean size of nanocrystals. From the XRD diffraction pattern observed for nanoparticles, the Scherrer equation was applied to calculate the crystallite size.

The results of the XRD examination show that the Cu-NPs that were created had a structure with a face-centered cubic (FCC) with a lattice constant of 0.36 nanometers that matches well with the standard lattice parameter (a = 0.3615 nanometers). JCPDS card no, 04-0836, the average size of copper crystals and cu@sio2 nanoparticles(D) calculated by using equ.1, the Scherrer equation were about 47.08 and 58.9 respectively [21].

https://doi.org/10.17993/3ctecno.2023.v12n1e43.337-352

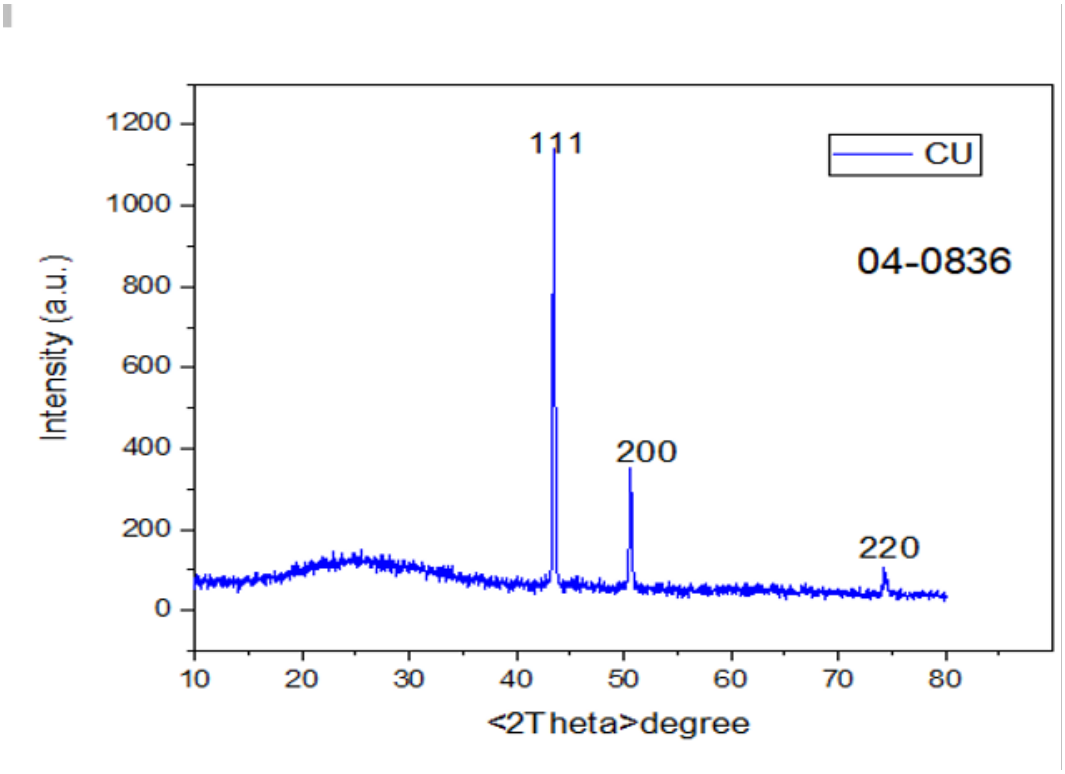

Figure 1. XRD patterns of CuNps

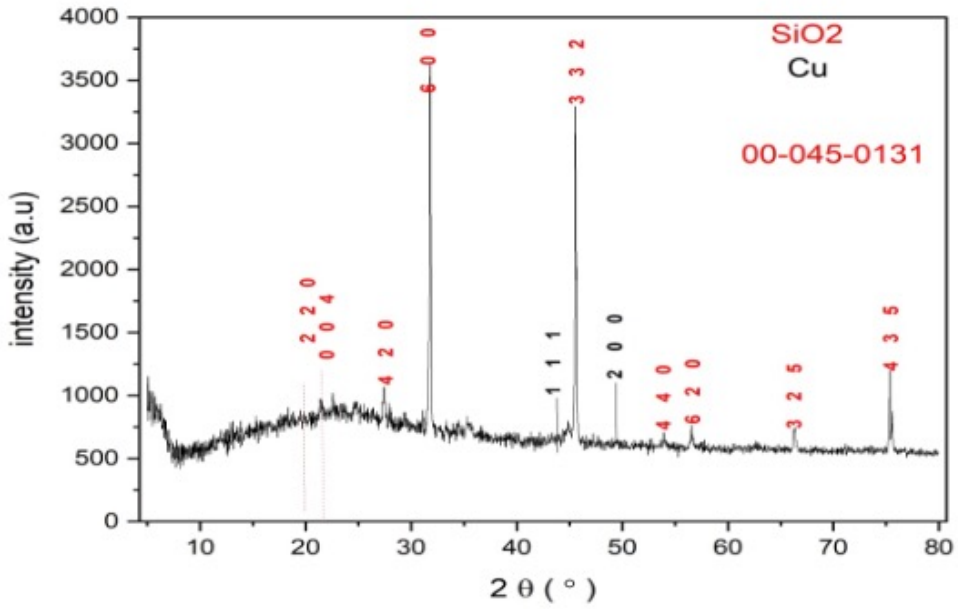

Figure 2. XRD patterns of silica-coated Cu nanoparticles

3.2. UV VISIBLE SPECTROSCOPY

Small metallic nanoparticles exhibit visible electromagnetic wave absorption through surface-based collective conduction electron oscillation [18]. The surface plasmon resonance effect is what's happening here. The advantage of this effect is that it can be used as a tracer for the presence of metallic nanoparticles with a

https://doi.org/10.17993/3ctecno.2023.v12n1e43.337-352

straightforward UV-visible spectrometer, as demonstrated by the size dependence of the plasmonic resonance of the absorption of copper nanoparticles and core-shell particles of copper / silica prepared by chemical sol-gel method.The results from UV-visible demonstrate a red shift in the absorption spectra caused by the increase in particle size caused by the increased silica coating that the synthesis of $Cu@SiO_2$ nanostructure exhibited in the figure displayed SPR peak at 635 nanometer, when it was at the wavelength of 630 nanometer for cu nanoparticles. Fig:3

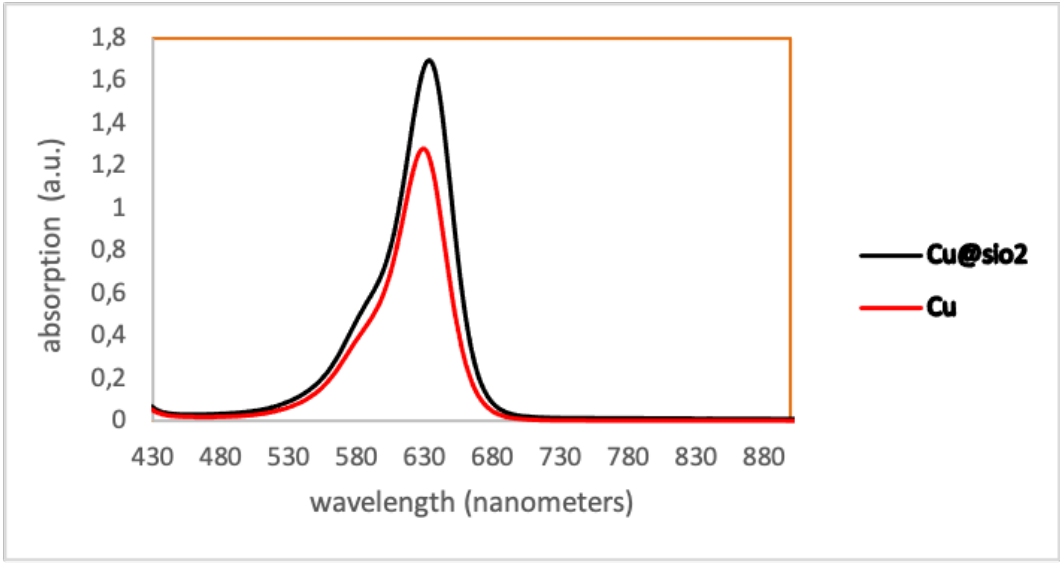

Figure 3. UV-vis absorption spectra for Cu and Cu @Sio2

3.3. FTIR

The FTIR spectra of silica (Sio_2) fig:3a and 3b Cu @ Sio_2 .The wide band at 3356 cm^{-1} in the FTIR of Sio2 corresponds to the O-H stretching vibration. of the condensation of a silanol group (Si-OH) as well as the residual absorbed water in the FTIR spectra of SiO2 and Cu @ Sio2 in Figure. Water molecules' bending and vibrations as they absorbed into the surface of the silica particles caused a small peak at 1666 cm^{-1}. [22].

There were characteristic peaks at 1029 cm-1, 794 cm-1, and 474 cm-1, which represented, respectively, the bending oscillation of O-Si-O, the asymmetrical extending vibration of Si-O-Si, and the symmetric stretching vibration of O-Si-O [23]. The vibrations of the silanol groups stretching are connected with the band at 1029 cm^{-1},while the peak at 1396 cm^{-1} is connected to the stretching of the Si-O bond [22]. Similar to the Sio_2 spectrum, FTIR spectrum of cu @ sio_2 nanoparticles in Figure4b likewise showed typical vibrations, but peaks were displaced to a higher number of waves, such as peaks of 2916 cm^{-1} to 2920 cm^{-1},peaks between 1423 cm^{-1} and 1458 cm^{-1} as well as the peaks between 1639 and 1666 cm^{-1}. This bond can be seen at 1666 cm^{-1} before to the production of nanoparticles and has since migrated to 1639 cm^{-1}.

The results may confirm that the copper nanoparticles were synthesized and encapsulated with silica by the Stober's method; The change in wave numbers was

https://doi.org/10.17993/3ctecno.2023.v12n1e43.337-352

due to C=C stretching and reveals coordination with Cu nanoparticles. Moreover, FTIR peak in Fig. 4b indicates that a peak of 624 cm $^{-1}$ It may refer to copper nanoparticles [24- 26].

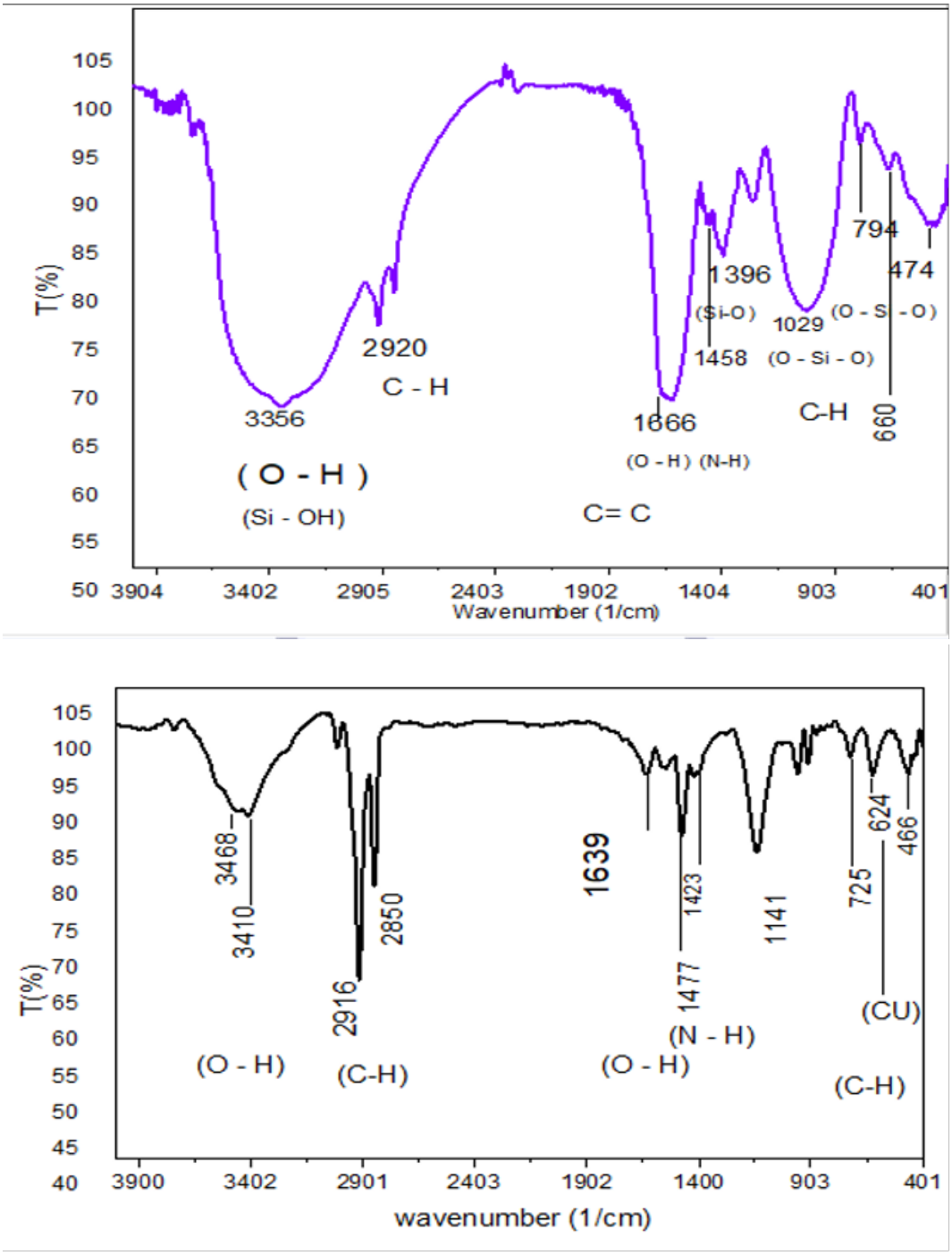

Figure 4. ftir spactra of a- Sio2 b- cu@Sio2

3.4. TEM.

The analyses of the TEM pictures are useful equipment for evaluating the size and form of the prepared nanoparticles. Fig. 4 displays common TEM pictures of cu@Sio2 NPs, their look is spherical in shape with a cover around them, as in Fig. 5, and they also offer a wide range of sizes cu @sio$_2$ core shell dimeter is between (35 and 120) nanometer and rate 66 nanometer as in the fig.6.

https://doi.org/10.17993/3ctecno.2023.v12n1e43.337-352

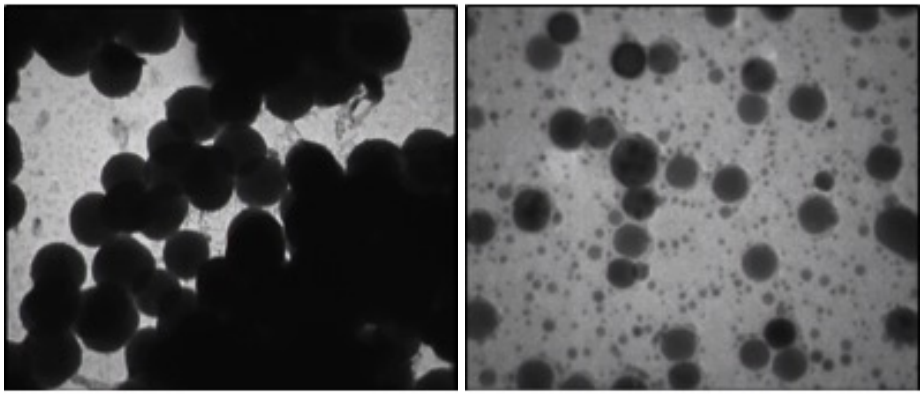

Figure 5. TEM images of Cu@Sio2 core shell NPs

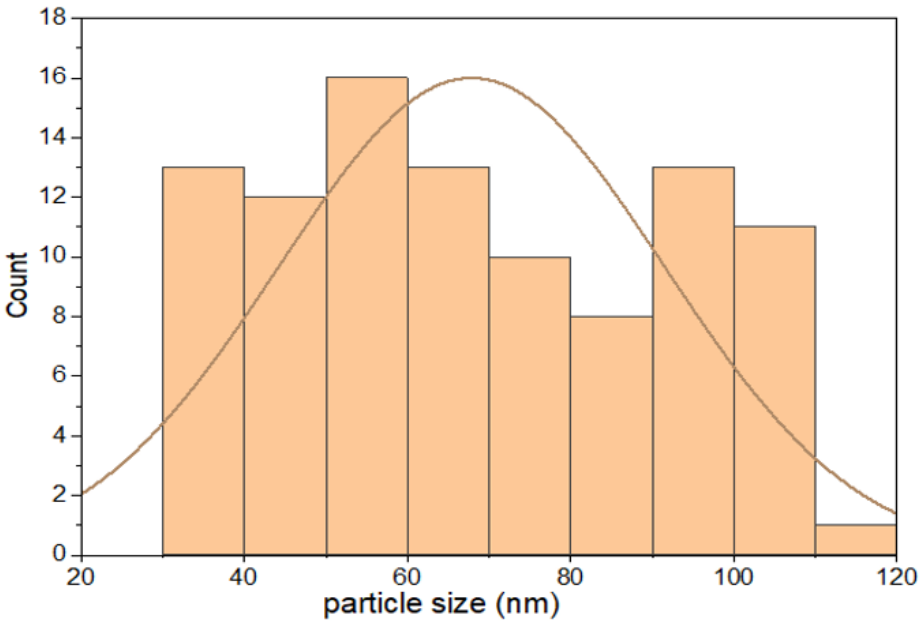

Figure 6. TEM Histograms of Cu@Sio2 core shell NPs

3.5. FESEM-EDX

By using feSEM-EDX analyses, the existence of Cu@sio$_2$ core-shell was established, and the outcome seems to show a spherical agglomeration in the particle size distribution, with diameters ranging from 80 to 184 nanometers. High magnification examination shows more details, though, including the fact that these copper nanoclusters are made up of smaller nanoparticles with good homogeneity, whose average diameter is roughly 152 nanometers (figs. 7 and 8 show this). The copper that was generated and the silica that it was coated in can both be clearly seen in the EDX analysis in Fig. 9. It should be noted that the copper-metal NPs were silicate-coated.

https://doi.org/10.17993/3ctecno.2023.v12n1e43.337-352

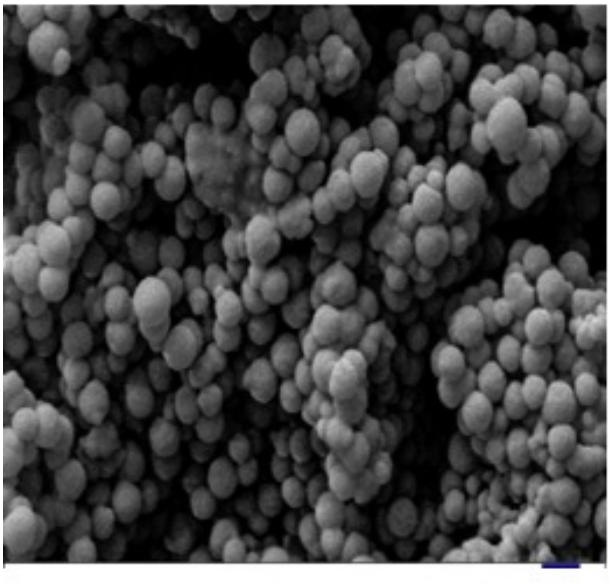

Figure 7. fesem showing the copper nanoparticle capping with silica

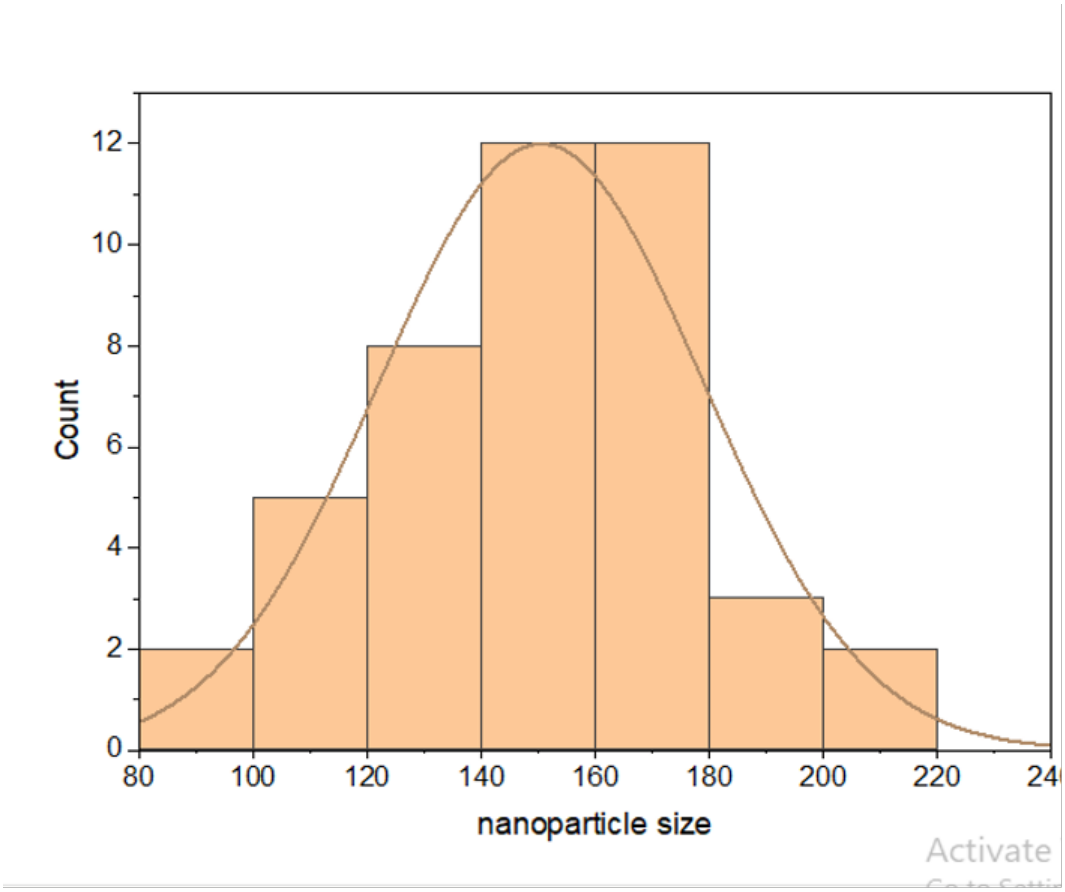

Figure 8. fesem Histograms of Cu@Sio2NPs

https://doi.org/10.17993/3ctecno.2023.v12n1e43.337-352

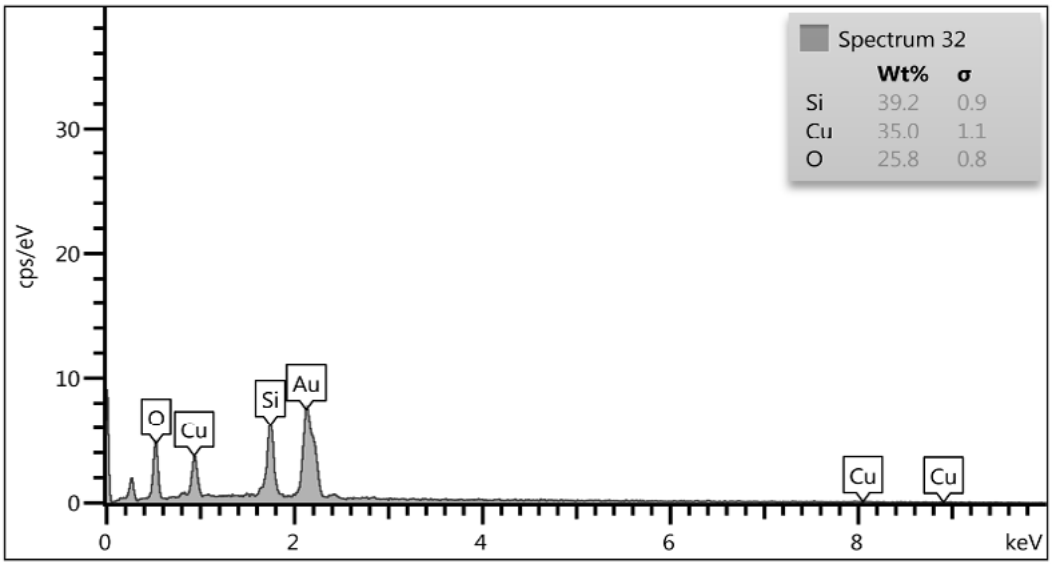

Figure 9. EDS Diagram showing the presence of copper Nps and silica

4. EVALUATION OF ANTIBACTERIAL

4.1. ACTIVITY OF THE CORE-SHELLS

Results of the evaluation of the antibacterial activity of the disc diffusion method prepared from core and shells in Figures (10) and (11) shows the inhibition region where the rate of bacterial reduction was for samples (14, 14, 16 and 20) for Escherichia coli and (24, 24, 28 and 30) for Staphylococcus aureus. Samples were taken with dilute concentrations (12.5, 25, 50, 100) %. They showed a high bacterial reduction rate for each Escherichia coli and Staphylococcus aureus in particular,

cu @sio2core shell, showed greater action against Staphylococcus aureus than their action against Escherichia coli, which was observed from the reduction rate after only 24 hours. The mechanisms by which copper is toxic to bacteria have been identified as the generation of free radicals [27, 28], which leads to the permeabilization of cell membranes, and the degradation of DNA and RNA. In the case of the antibacterial activity of free radicals, interactions with the proteins inside the bacteria in samples containing copper result in the production of hydroxyl radicals (OH) and peroxide anions (O_2). The resultant radicals damage DNA and RNA by degrading intracellular and extracellular components that obstruct the electron transport system. In addition, the eluted copper affects the bacterial outer membrane, creating holes in the outer membrane that are atypically formed. Changes in these membranes alter membrane permeability, leading to a gradual release of lipopolysaccharide molecules and membrane proteins, leading to the death of the bacteria [29].

The size, shape, and concentration of copper nanoparticles, as well as the synthesis procedure, all affect the antibacterial action of cu@sio2 core shell. The presence of the copper nanopowder coated by SiO2 was verified by TEM measurements of core shells made using the sol-gel method.Cu@Sio_2 nanoparticles

https://doi.org/10.17993/3ctecno.2023.v12n1e43.337-352

core - shell displayed sufficient performance as antibacterial agent. Although the presence of the SiO_2 shell prevented direct contact with the Cu nano powder, it still yielded high a reduction rate for bacteria. Thus, it was confirmed that an antibacterial agent capable of overcoming the disadvantages of using nanopowder could be manufactured. In addition, by controlling the thickness of the shell, the elution of Cu can be delayed and antibacterial functions can be maintained for long periods.

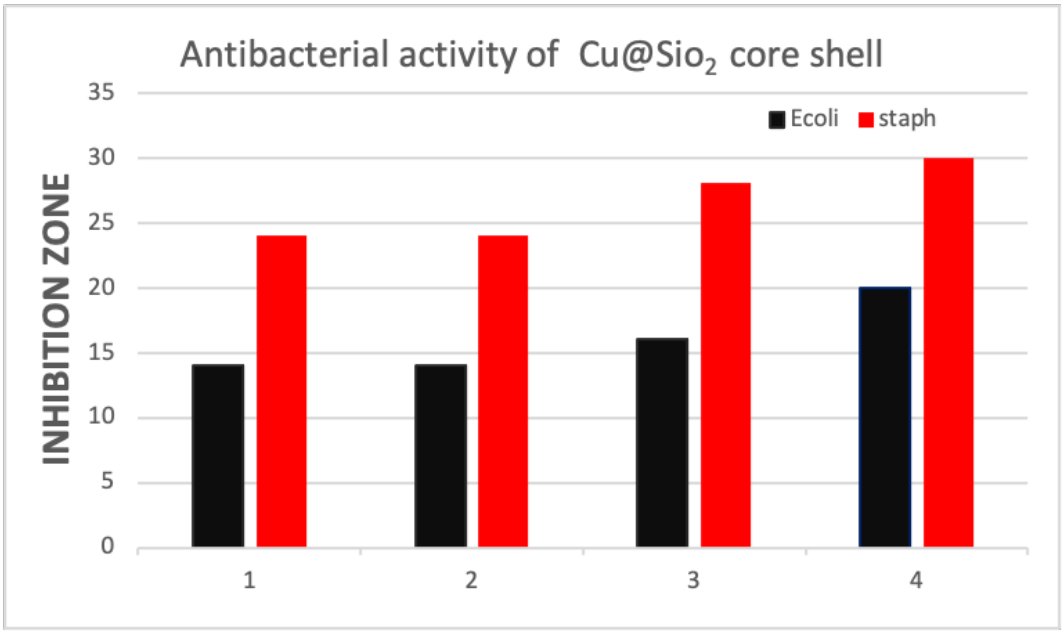

Figure 10. antibacterial activity of copper @sio2 core shell vs E.coli and S. aureus bacteria(the inhibition zone)

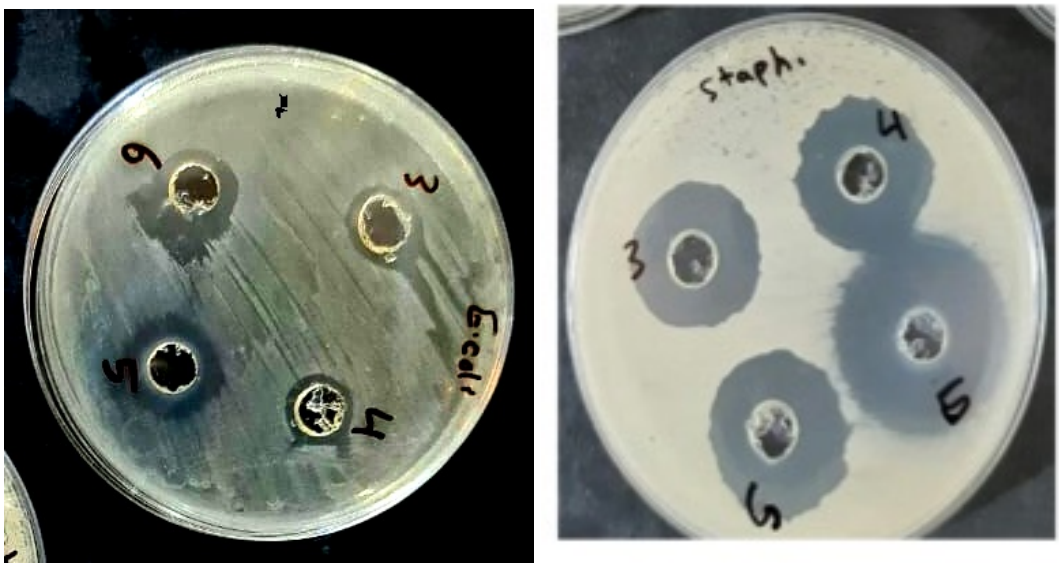

Figure 11. Cu@Sio2 core shell inhibition zone of E. coli and S. aureus bacteria at four diluted concentrations (12.5%, 25%, 50, and 100%)

5. CONCLUSIONS

A chemical sol-gel process was used to create CuSiO2 nanoparticles with a core-shell structure. A spherical sio_2 shell was formed using the sol-gel process, and Cu

https://doi.org/10.17993/3ctecno.2023.v12n1e43.337-352

nanopowder was present at the center. The presence of ammonia was also confirmed as being essential to the process. Using the shaking flask method, the spectra of xrd confirm the presence of copper nanoparticles, and the Fesem and Tem images confirm the formation of spherical particles. A red shift was observed in the UV-vis absorption spectra, indicating an increase in particle size, and it was confirmed that the core-shells produced through sol-gel method exhibited antibacterial activity. Cu@sio$_2$ core-shell can be used as a futuristic, effective antibacterial agent in biomedical applications.

REFERENCES

(1) Chauhan, S., Kumar, M., Chhoker, S., & Katyal, S. C. (2016). **A comparative study on structural, vibrational, dielectric and magnetic properties of microcrystalline BiFeO3, nanocrystalline BiFeO3 and core–shell structured BiFeO3@ SiO2 nanoparticles**. *Journal of Alloys and Compounds*, 666, 454-467..

(2) Fang, L., Wu, W., Huang, X., He, J., & Jiang, P. (2015). **Hydrangea-like zinc oxide superstructures for ferroelectric polymer composites with high thermal conductivity and high dielectric constant**. *Composites Science and Technology*, 107, 67-74.

(3) Zhou, W., Chen, Q., Sui, X., Dong, L., & Wang, Z. (2015). **Enhanced thermal conductivity and dielectric properties of Al/β-SiCw/PVDF composites**. *Composites Part A: Applied Science and Manufacturing*, 71, 184-191.

(4) Wen, F., Liu, X., Xu, Z., Tang, H., Bai, W., Zhao, W. S., ... & Wang, G. (2017). L**ow loss and high permittivity composites based on poly (vinylidene fluoride-chlorotrifluoroethylene) and lead lanthanum zirconate titanate**. *Ceramics International*, 43(1), 1504-1508.

(5) Janardhanan, R., Karuppaiah, M., Hebalkar, N., & Rao, T. N. (2009). **Synthesis and surface chemistry of nano silver particles**. *Polyhedron*, 28(12), 2522-2530.

(6) Bhattacharyya, S., Kudgus, R. A., Bhattacharya, R., & Mukherjee, P. (2011). **Inorganic nanoparticles in cancer therapy**. Pharmaceutical research, 28, 237-259.

(7) Tiquia-Arashiro, S., & Rodrigues, D. F. (2016). **Extremophiles: applications in nanotechnology** (p. 193). *New York, NY, USA:: Springer International Publishing.*

(8) Bhatia, S. (2016). **Natural polymer drug delivery systems: Nanoparticles, plants, and algae**. *Springer*.

(9) Singh, R., & Nalwa, H. S. (2011). **Medical applications of nanoparticles in biological imaging, cell labeling, antimicrobial agents, and anticancer nanodrugs**. *Journal of biomedical nanotechnology*, 7(4), 489-503. https://doi.org/10.1166/jbn.2011.1324.

(10) Cuffari B. (2017). Nanotechnology in the Paint Industry. https://www.azonano.com/article.aspx?ArticleID=4710.

https://doi.org/10.17993/3ctecno.2023.v12n1e43.337-352

(11) Santhoshkumar, J., Agarwal, H., Menon, S., Rajeshkumar, S., & Kumar, S. V. (2019). **A biological synthesis of copper nanoparticles and its potential applications**. *Green Synthesis, Characterization and Applications of Nanoparticles* (pp. 199-221). Elsevier.

(12) Kırmusaoğlu, S. (Ed.). (2019). **Antimicrobials, Antibiotic Resistance, Antibiofilm Strategies and Activity Methods**. BoD–Books on Demand.

(13) Agarwala, M., Choudhury, B., & Yadav, R. N. S. (2014). **Comparative study of antibiofilm activity of copper oxide and iron oxide nanoparticles against multidrug resistant biofilm forming uropathogens**. *Indian journal of microbiology*, 54, 365-368. https://doi.org/10.1007/s12088-014-0462-z.

(14) Chaudhary, J., Tailor, G., Yadav, B. L., & Michael, O. (2019). **Synthesis and biological function of Nickel and Copper nanoparticles**. *Heliyon*, 5(6), e01878. https://doi.org/10.1016/j.heliyon.2019.e01878

(15) Mary, A. A., Ansari, A. T., & Subramanian, R. (2019). **Sugarcane juice mediated synthesis of copper oxide nanoparticles, characterization and their antibacterial activity**. *Journal of King Saud University-Science*, 31(4), 1103-1114. https://doi.org/10.1016/j.jksus.2019.03.003

(16) Ismail, M. I. M. (2020). **Green synthesis and characterizations of copper nanoparticles**. *Materials Chemistry and Physics*, 240, 122283. https://doi.org/10.1016/j.matchemphys.2019.122283

(17) Harishchandra, B. D., Pappuswamy, M., Antony, P. U., Shama, G., Pragatheesh, A., Arumugam, V. A., ... & Sundaram, R. (2020). **Copper nanoparticles: a review on synthesis, characterization and applications**. *Asian Pacific Journal of Cancer Biology*, 5(4), 201-210. ,https://doi.org/10.31557/APJCB.2020.5.4.201

(18) Trapalis, C. C., Kokkoris, M., Perdikakis, G., & Kordas, G. (2003). **Study of antibacterial composite Cu/SiO2 thin coatings**. *Journal of sol-gel science and technology*, 26(1-3), 1213-1218.

(19) Ghosh Chaudhuri, R., & Paria, S. (2012). **Core/shell nanoparticles: classes, properties, synthesis mechanisms, characterization, and applications**. *Chemical reviews*, 112(4), 2373-2433.

(20) Hu, W., Chen, S., Li, X., Shi, S., Shen, W., Zhang, X., & Wang, H. (2009). **In situ synthesis of silver chloride nanoparticles into bacterial cellulose membranes**. *Materials Science and Engineering: C*, 29(4), 1216-1219.

(21) Mishra, G., Verma, S. K., Singh, D., Yadawa, P. K., & Yadav, R. R. (2011). **Synthesis and ultrasonic characterization of Cu/PVP nanoparticles-polymer suspensions**. *Open Journal of Acoustics*, 1(01), 9.

(22) Martınez, J. R., Ruiz, F., Vorobiev, Y. V., Pérez-Robles, F., & González-Hernández, J. (1998). **Infrared spectroscopy analysis of the local atomic structure in silica prepared by sol-gel**. *The Journal of chemical physics*, 109(17), 7511-7514.

(23) Furlan, P. Y., Furlan, A. Y., Kisslinger, K., Melcer, M. E., Shinn, D. W., & Warren, J. B. (2019). **Water as the solvent in the stober process for forming ultrafine silica shells on magnetite nanoparticles**. *ACS Sustainable Chemistry & Engineering*, 7(18), 15578-15584.

https://doi.org/10.17993/3ctecno.2023.v12n1e43.337-352

(24) Selvaraj, M., Sinha, P. K., Lee, K., Ahn, I., Pandurangan, A., & Lee, T. G. (2005). **Synthesis and characterization of Mn–MCM-41and Zr–Mn-MCM-41**. *Microporous and mesoporous materials*, 78(2-3), 139-149.

(25) Díaz-Visurraga, J., Daza, C., Pozo, C., Becerra, A., von Plessing, C., & García, A. (2012). **Study on antibacterial alginate-stabilized copper nanoparticles by FT-IR and 2D-IR correlation spectroscopy**. *International Journal of Nanomedicine*, 3597-3612.

(26) Ridzuan, R., Maksudur Rahman, K., Najmul Kabir, C., Mohammad Dalour Hossen, B., Rohaya Mohamed, H., Astimar Abdul, A., ... & Nahrul Hayawin, Z. (2013). **Development of Cu nanoparticle loaded oil palm fibre reinforced nanocomposite**. *Advances in Nanoparticles*, 2013.

(27) Sani, A., Cao, C., & Cui, D. (2021). **Toxicity of gold nanoparticles (AuNPs): A review**. *Biochemistry and biophysics reports*, 26, 100991.

(28) Das, S., Debnath, N., Mitra, S., Datta, A., & Goswami, A. (2012). **Comparative analysis of stability and toxicity profile of three differently capped gold nanoparticles for biomedical usage**. *Biometals*, 25, 1009-1022.

(29) Jafari, M., Rokhbakhsh-Zamin, F., Shakibaie, M., Moshafi, M. H., Ameri, A., Rahimi, H. R., & Forootanfar, H. (2018). **Cytotoxic and antibacterial activities of biologically synthesized gold nanoparticles assisted by Micrococcus yunnanensis strain J2**. *Biocatalysis and agricultural biotechnology*, 15, 245-253.

https://doi.org/10.17993/3ctecno.2023.v12n1e43.337-352